

Single crystal growth and anisotropic magnetic properties of HoAl_2Ge_2

Md. Matin, Rajib Mondal, A. Thamizhavel, A. Provino, P. Manfrinetti, and S. K. Dhar

Citation: *AIP Advances* **8**, 055709 (2018);

View online: <https://doi.org/10.1063/1.5007158>

View Table of Contents: <http://aip.scitation.org/toc/adv/8/5>

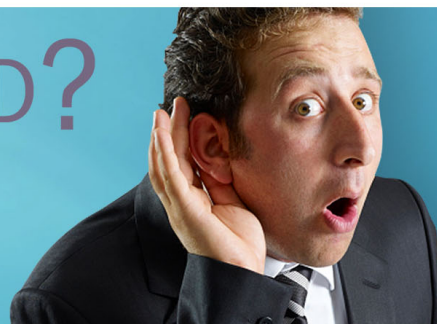
Published by the [American Institute of Physics](#)

HAVE YOU HEARD?

Employers hiring scientists and
engineers trust

PHYSICS TODAY | JOBS

www.physicstoday.org/jobs



Single crystal growth and anisotropic magnetic properties of HoAl_2Ge_2

Md. Matin,¹ Rajib Mondal,¹ A. Thamizhavel,¹ A. Provino,^{2,3} P. Manfrinetti,^{2,3} and S. K. Dhar^{1,a}

¹Department of Condensed Matter Physics and Materials Science, TIFR, Mumbai 400005, India

²Department of Chemistry, University of Genova, Via Dodecaneso 31, 16146 Genova, Italy

³Institute SPIN-CNR, Corso Perrone 24, 16152 Genova, Italy

(Presented 9 November 2017; received 30 September 2017; accepted 11 November 2017; published online 28 December 2017)

We have grown a single crystal of HoAl_2Ge_2 , which crystallizes in the hexagonal CaAl_2Si_2 type structure with Ho ions in the trigonal coordination in the ab plane. The data obtained from the bulk measurement techniques of magnetization, heat capacity and transport reveal that HoAl_2Ge_2 orders antiferromagnetically at $T_N \sim 6.5$ K. The susceptibility below T_N and isothermal magnetization at 2 K indicate the ab plane as the easy plane of magnetization. Heat capacity data reveal a prominent Schottky anomaly with a broad peak centered around 25 K, suggesting a relatively low crystal electric field (CEF) splitting. The electrical resistivity reveals the occurrence of a superzone gap below T_N . The point charge model of the CEF is applied to the magnetization and the heat capacity data. While a good fit to the paramagnetic susceptibility is obtained, the CEF parameters do not provide a satisfactory fit to the isothermal magnetization at 2 K and the Schottky anomaly. © 2017 Author(s). All article content, except where otherwise noted, is licensed under a Creative Commons Attribution (CC BY) license (<http://creativecommons.org/licenses/by/4.0/>). <https://doi.org/10.1063/1.5007158>

INTRODUCTION

The family of rare earth compounds RAl_2Ge_2 is known to form for $\text{R} = \text{Y}, \text{La-Nd}, \text{Sm-Lu}$, including Eu and Yb^{1} in the hexagonal CaAl_2Si_2 prototype (Pearson symbol $hP5$, space group $P\bar{3}m1$, No. 164; $Z = 1^2$); this prototype is also cited and reported as Ce_2SO_2 -type.³ The unit cell shows three inequivalent Wyckoff sites, the R atoms occupy the $1a$ site, while Al and Ge atoms fill the two different $2d$ sites, respectively. A sketch of the unit cell is shown in Fig. 1. The rare earth ions form a net on the ab -plane with trigonal coordination.

The magnetic properties of polycrystalline RAl_2X_2 ($\text{R} = \text{Eu}$ and Yb ; $\text{X} = \text{Si}$ and Ge) have been reported earlier in literature.^{4,5} Iso-structural EuAl_2Si_2 and EuAl_2Ge_2 order antiferromagnetically at $T_N = 35.5$ and 27.5 K, respectively. The ^{151}Eu Mössbauer spectra are in conformity with the divalent nature of Eu ions in these two compounds. YbAl_2Si_2 has been reported to be a valence fluctuating compound, while iso-structural YbAl_2Ge_2 is a simple Pauli paramagnet characterized by a non-magnetic, divalent state of Yb ions. Anisotropic magnetization at 2 K was reported in a single crystal of EuAl_2Si_2 , which was rather unexpected as Eu^{2+} ion is an S-state ion⁶ with negligible magnetocrystalline anisotropy. As noted above, the rare earth ions in RAl_2Ge_2 are trigonally coordinated in the ab -plane. An antiferromagnetic exchange interaction between the rare earth ions may give rise to possible frustration effects. Therefore, it is of interest to study the magnetic behavior of these compounds. In this work, we report the magnetic properties of a single crystal of HoAl_2Ge_2 , using magnetization, heat capacity and electrical transport measurements.

^aCorresponding Author E-mail: sudesh@tifr.res.in (Sudesh Kumar Dhar)

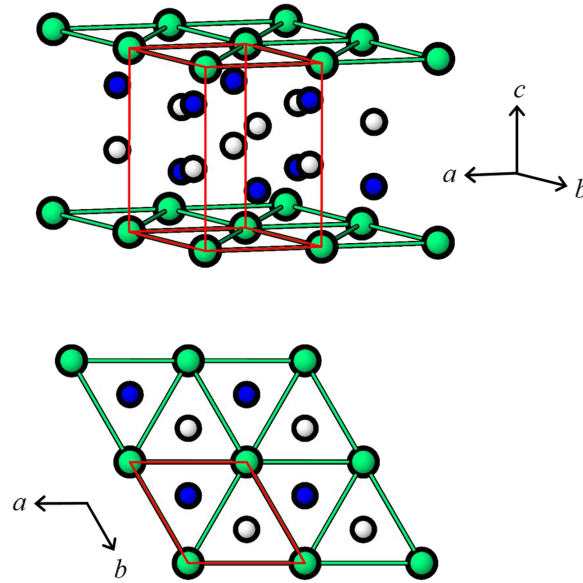


FIG. 1. Sketch of the crystal structure of HoAl_2Ge_2 where the shortest Ho-Ho interatomic distances on the ab -plane are highlighted (Ho atoms in green, Al atoms in white and Ge atoms in blue).

EXPERIMENTAL DETAILS

The single crystals of HoAl_2Ge_2 were prepared by the flux method, using Al-Ge eutectic composition as flux. A polycrystalline sample of HoAl_2Ge_2 was taken together with Al-Ge flux in the ratio of 1:19 in an alumina crucible placed within an evacuated quartz tube and heated up to 1100°C . After homogenization for 24 hours the solution was gradually cooled at the rate of $2^\circ\text{C}/\text{hour}$. The contents were centrifuged at 600°C resulting in the formation of single crystals of HoAl_2Ge_2 of typical planar dimensions of $\sim 4\text{ mm} \times 2\text{ mm}$. The crystal symmetry of a single crystal specimen was checked on a Bruker-Nonius MACH3 diffractometer, using graphite-monochromated $\text{Mo K}\alpha$ radiation. Few single crystals were crushed to powder for recording a powder diffraction pattern using $\text{CuK}\alpha$ radiation. Magnetization was recorded on MPMS SQUID and VSM magnetometers, while heat capacity and the electrical transport were measured on a PPMS (Quantum Design, U.S.A.).

RESULTS AND DISCUSSION

The lattice parameters for HoAl_2Ge_2 as obtained from single crystal diffraction data are $a = 4.191(1)\text{ \AA}$ and $c = 6.653(1)\text{ \AA}$. The shortest Ho-Ho distance is 4.191 \AA (the a -axis) while the next larger Ho-Ho distance is 6.653 \AA (the c -axis). These distances are larger than the Ho-Ho bond distance of 3.532 \AA , based on the sum of two metallic radii of Ho ion.⁷ The powder diffraction pattern could be indexed based on the symmetry type of CaAl_2Si_2 and the lattice parameters inferred from the single crystal data. The spectrum did not show the presence of any extra peaks due to the parasitic impurity phases, confirming the phase purity of the grown crystals.

The inverse susceptibility $\chi^{-1}(T)$ measured in an applied field of 3 kOe is plotted as a function of temperature in Fig. 2(a). A fit of the Curie-Weiss formula $\chi(T) = C/(T - \theta_p)$ to $\chi(T)$ data above 150 K gives the paramagnetic Curie temperature $\theta_p = -7.4$ and -4.2 K , and the effective paramagnetic moment $\mu_{\text{eff}} = 10.61$ and $10.92\text{ } \mu_B/\text{Ho}$ for field applied along the c -axis and the basal ab plane, respectively. The negative value of θ_p implies the antiferromagnetic nature of the magnetic interaction between the localized $4f$ Ho moments. The experimentally obtained values of μ_{eff} are close to the Hund's rule derived free ion value of $10.6\text{ } \mu_B/\text{Ho}$ for the $4f^{10}$ configuration of Ho.

The upper and lower insets of Fig. 2(a) show $\chi(T)$ at selected fields below 20 K for $H \parallel ab$ and $H \parallel c$, respectively. The observed higher value of $\chi(T)$ for $H \parallel ab$ than that for $H \parallel c$ implies that in HoAl_2Ge_2 the basal plane is the easy plane of magnetization. Susceptibility measured at 100 Oe

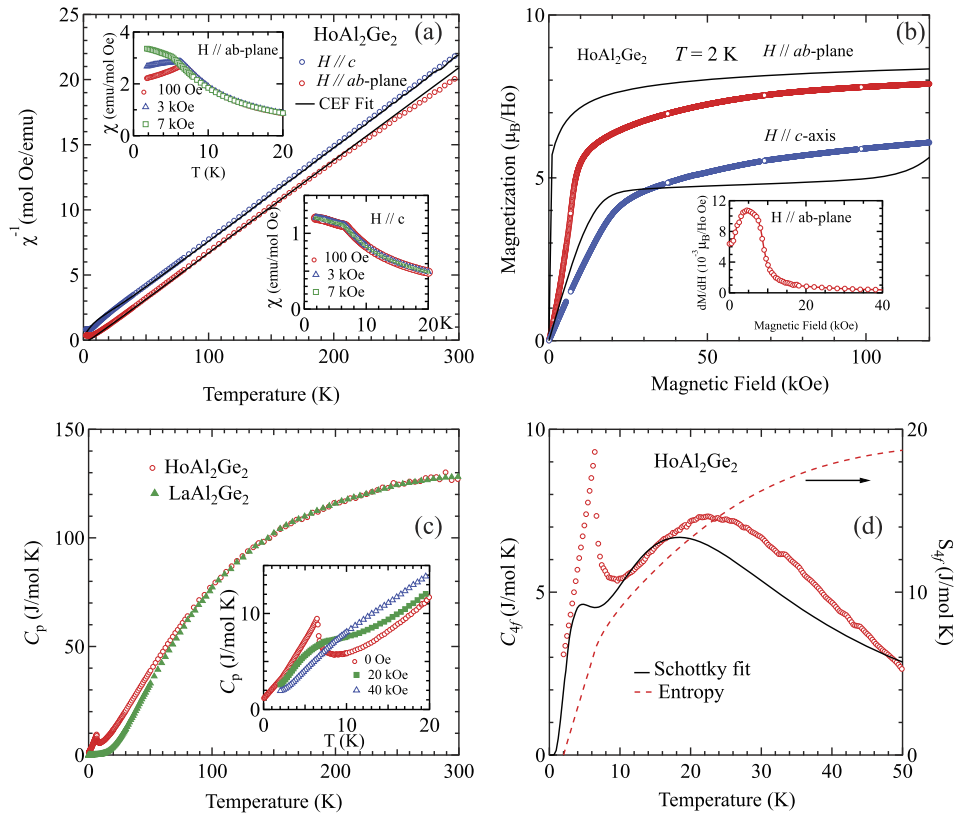


FIG. 2. (a) Temperature variation of inverse magnetic susceptibility data of HoAl_2Ge_2 along the two principal crystallographic directions. The solid line is the fit based on CEF calculations. Insets show the temperature variation of dc magnetic susceptibility of HoAl_2Ge_2 along ab -plane and c -direction at various applied magnetic fields. (b) Magnetization vs. field at 2 K of HoAl_2Ge_2 and the solid line is calculated data based on CEF calculations. (c) Temperature dependent heat capacity of HoAl_2Ge_2 and LaAl_2Ge_2 . Inset shows the temperature variation of heat capacity of HoAl_2Ge_2 in various applied magnetic fields. (d) Temperature variation of the $4f$ -derived heat capacity and the corresponding entropy of HoAl_2Ge_2 and the solid line is the calculated Schottky heat capacity based on CEF calculations.

field applied along the basal plane passes through a maximum at $T_N \sim 6.7$ K, indicating the onset of long-range antiferromagnetic ordering of the Ho moments. As the field is increased to 3 kOe and further to 7 kOe the T_N shifts to lower temperatures and $\chi(T)$ below T_N shows significant field dependence. On the other hand, $\chi(T)$ for the field along the c axis shows a mild kink at T_N , increases marginally below T_N , and shows no perceptible field dependence. The ratio of θ_p/T_N is ~ 1 , indicating the absence of geometrically induced exchange frustration in the trigonally coordinated Ho ions. In systems with appreciable frustration the ratio is typically several times larger than unity. We may note here that in the iso-structural EuAl_2Si_2 , it was found from neutron diffraction that the Eu magnetic moments are ferromagnetically coupled in the ab -plane while they are antiferromagnetically coupled along the trigonal axis.⁴

Figure 2(b) shows isothermal magnetization $M(H)$ curves at 2 K for both field orientations. $M(H)$ data clearly reveal that the basal plane is the easy plane of magnetization, which is in agreement with the data of the temperature variation of magnetic susceptibility [Insets of Fig. 2(a)]. Magnetization along the basal plane increases rapidly with increasing field up to ~ 10 kOe. The variation of magnetization with field becomes gradually slower for fields above 10 kOe, but magnetization does not saturate even at the highest applied field (here 140 kOe) to the free-ion value of $10 \mu_B$ ($g_J J$). A close inspection of the low-field, in-plane $M(H)$ data reveals that the magnetization displays a metamagnetic transition at the critical field $H_c \sim 4.7$ kOe [determined from the peak position of the dM/dH versus H curve (inset of Fig. 2(b))], indicating a spin reorientation. The effect of this field-induced spin reorientation is reflected in the $M(T)$ plots in different constant fields shown in the upper inset of

Fig. 2(a). In the low-field regime the peak position in $M(T)$ corresponds to the AFM phase transition temperature T_N , which shifts to low temperatures as the field is increased, and almost disappears at field close to H_c . For field above H_c , $M(H)$ displays characteristics similar to that of a ferromagnet. The overall trend of $M(H)$ for field along the c axis is qualitatively similar to that for field along the basal plane except that in the former case no metamagnetic transition is observed and the magnetization at all fields is less than the corresponding value for $H // ab$. The temperature dependence of $M(T)$ for $T < T_N$ indicates that the magnetic configuration of Ho ions in HoAl_2Ge_2 differs from that of a bipartite collinear antiferromagnet for which $\chi //$ decreases to zero as T approaches absolute zero and χ_{\perp} is temperature independent for $T < T_N$. A similar conclusion is also drawn from $M(H)$ plots at 2 K.

The main panel of Fig. 2(c) shows the heat capacity, C_p , of HoAl_2Ge_2 and non-magnetic, reference LaAl_2Ge_2 up to 300 K. It may be noted that the heat capacity of both compounds at 300 K attains the value of $3nR$ (R is the gas constant) with $n = 5$. The inset shows the data below 20 K for HoAl_2Ge_2 in zero field and in applied fields of 20 and 40 kOe. The heat capacity of HoAl_2Ge_2 exhibits a λ -type peak at ~ 6.6 K, confirming the bulk magnetic transition of the Ho ions. The zero-field data for HoAl_2Ge_2 were measured down to ~ 0.4 K. The zero-field anomaly at 6.6 K is significantly altered in applied fields of 20 and 40 kOe, qualitatively in conformity with the $M(T)$ data shown in the upper inset of Fig. 2(a). For LaAl_2Ge_2 , C_p/T versus T^2 is linear below ~ 8 K and a fit of the expression $C_p/T = \gamma + \beta T^2$ to the data results in an electronic specific heat coefficient $\gamma = 5$ mJ/mol K². A value of 306 K for the Debye temperature θ_D is inferred from the lattice heat capacity coefficient β . An estimate of $4f$ -derived heat capacity C_{4f} in HoAl_2Ge_2 can be obtained by subtracting the heat capacity of LaAl_2Ge_2 from that of HoAl_2Ge_2 , making the usual assumption that the phonon heat capacities in the two compounds are same after taking account of the slightly different atomic masses of La and Ho. The plot of C_{4f} and the corresponding entropy S_{4f} is shown in Fig. 2(d). C_{4f} shows a very prominent broad peak centered around 25 K, which is attributed to the Schottky heat capacity. The relatively low value of the peak temperature suggests that the CEF splitting in HoAl_2Ge_2 is low as the Schottky anomaly arises due to the changing values of the fractional occupation of the CEF-split levels with temperature. The $4f$ -derived entropy S_{4f} attains a value of 1.53 R at T_N , which substantially exceeds the entropy $R \ln 2$ (0.693 R) for spin-half, $S = 1/2$ level. This suggests the presence of several low-lying crystal field levels below T_N in HoAl_2Ge_2 .

The electrical resistivity with the current density $J // ab$ -plane, shown in Fig. 3 displays normal metallic behavior. The resistivity below 25 K, plotted in the inset of Fig. 3, shows an upturn below ~ 9 K indicating the existence of antiferromagnetic correlations in the paramagnetic regime close to T_N and the occurrence of a super zone gap below T_N .

We have applied the point-charge CEF model to the magnetization and heat capacity data to get a semi-quantitative estimate of the CEF splitting. For the sake of simplicity, we performed the calculations assuming a hexagonal point symmetry for the rare earth Ho, though actually the $1a$ site possesses $-3m$ trigonal point symmetry. The 17 degenerate levels of the free Ho^{3+} ion ($J = 8$) are split into 11 levels by the hexagonal CEF potential. The CEF Hamiltonian for the hexagonal site symmetry is given by, $\mathcal{H}_{CEF} = B_2^0 O_2^0 + B_4^0 O_4^0 + B_6^0 O_6^0 + B_6^6 O_6^6$, where B_l^m are the crystal field parameters and O_l^m are the Stevens operator matrices. By diagonalizing the CEF Hamiltonian, using the eigenvalues and eigenfunctions, we have calculated the CEF susceptibility as shown in Fig. 2(a). The crystal field parameters thus obtained for a reasonably good fitting to the magnetic susceptibility are $B_2^0 = 4.5 \times 10^{-2}$ K, $B_4^0 = 9.9 \times 10^{-4}$ K, $B_6^0 = -1.99 \times 10^{-5}$ K and $B_6^6 = 8.99 \times 10^{-5}$ K with the molecular field constant -0.3 mol/emu for $H // c$ and 0.4 for $H // ab$ -plane. The present set of CEF parameters do not reproduce well the isothermal magnetization measured at 2 K Fig. 2(b). We can exclude magnetic frustration as a possible reason as the Curie-Weiss temperature and the magnetic transition temperature are of similar magnitude. Apparently, a more sophisticated model is required to provide a better description. For example, in the iso-structural EuAl_2Si_2 , in which the Eu ions are divalent and the effects of the CEF on the S -state Eu ions are negligible to first order, the authors had to assume three exchange interactions to explain their results.⁴ The obtained energy levels are 0 (2), 7, 13 (2), 37, 42 (2), 51, 55, 59 (2), 83 (2), 95 (2) and 101 K, the two in the parenthesis indicates a doublet state. These energy levels were used to estimate the Schottky heat capacity contribution to C_{4f} which is also plotted in Fig. 2(d). The mismatch between the calculated Schottky heat capacity

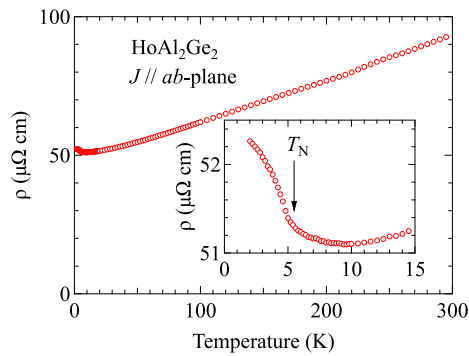


FIG. 3. Temperature variation of electrical resistivity of HoAl_2Ge_2 . Inset shows the enlarged view of the plot in the low temperature regime.

may be due to various reasons like the over simplified point charge model, or the assumption of identical phonon contribution in the Ho and La analogs, or assuming the infinitely sharp CEF levels, etc. However, the CEF analysis certainly points to a relatively low CEF splitting in HoAl_2Ge_2 .

To conclude we have explored the magnetic behavior of HoAl_2Ge_2 in which the Ho ions form triangular nets in the *ab*-plane. The compound orders at ~ 6.7 K with apparently no signature of frustration. The point charge CEF model was applied to the data but the parameters obtained do not reproduce well the isothermal magnetization at 2 K and the Schottky contribution to the heat capacity. This necessitates a more sophisticated model to explain the observed data.

¹ P. Villars and K. Cenzual, in *Pearson's Crystal Data-Crystal Structure Database for Inorganic Compounds*; ASM International, Materials Park, OH, USA, Release 2016/17. (Pearson's CD).

² C. Kranenberg, D. Johrendt, and A. Mewis, *Solid State Sci.* **4**, 261 (2002).

³ O. S. Zarechnyuk, A. A. Muravvova, and E. I. Gladyshevskii, *Dopov. Akad. Nauk Ukr. RSR Ser. A* **32**, 753 (1970).

⁴ P. Schobinger-Papamantellos and F. Hulliger, *J. Less-Common Met.* **146**, 327 (1989).

⁵ C. Kranenberg, D. Johrendt, A. Mewis, R. Pöttgen, G. Kotzyba, C. Rosenhahn, and B. D. Mosel, *Solid State Sciences* **2**, 215 (2000).

⁶ A. Maurya, R. Kulkarni, A. Thamizhavel, P. Bonville, and S. K. Dhar, *Journal of Physics: Conference Series* **592**, 012045 (2015).

⁷ E. Teatum, K. A. Gschneidner, Jr., and J. Waber, Rep LA-4003, NTIS, Springfield, VA, 1968.